Modeling of Casting, Welding and Advanced Solidification Processes X
Edited by D.M. Stefanescu, J. Warren, M. Jolly and M. Krane
TMS (The Minerals, Metals & Materials Society), 2003

MODELING THE DECOMPOSITION AND MICROSTRUCTURE EVOLUTION DURING SOLIDIFICATION OF HYPERMONOTECTIC ALLOYS

M. Wu[1], A. Ludwig[1], L. Ratke[2]

[1]Foundry Institute, Aachen University, Intzestr. 5, D-52072 Aachen, Germany;
[2]Institute for Space Simulation, DLR, D-51140 Cologne, Germany

Abstract

A new two phase model is developed to simulate the decomposition and microstructure evolution during solidification of hypermonotectic alloys. The minority liquid phase, decomposed from the parent melt as droplets, is treated as the second phase L_2, while the parent melt including the solidified monotectic matrix as the first phase L_1. The transport equations of mass, momentum, solute and enthalpy for both phases, and an additional conservation equation for the droplets are solved. Nucleation of the droplets, diffusion controlled growth, interphase interactions such as Marangoni (thermocapillary) force, Stokes force, solute partitioning and heat release of decomposition etc. are modeled by corresponding source and exchange terms in the conservation equations. The monotectic reaction is modeled by adding the latent heat on L_1 phase and applying suitable large viscosity to the solidified monotectic matrix. Simulation results of a square casting with hypermonotectic composition (Al-10wt.%Bi) under normal terrestrial condition and without gravity are presented.

Introduction

Alloys with a miscibility gap in liquid state, especially for those with gross composition beyond the monotectic point (hypermonotectic), are potential bearing materials for automotive industry[1-2]. A coarse spatial separation of the minority phase from the parent melt seems unavoidable no matter whether the alloy solidifies under normal terrestrial condition[3] or under reduced gravity situation[4-5]. Two mechanisms are responsible for this phenomenon: the gravity induced sedimentation and the Marangoni (thermocapillary) motion. Studies in last decades focused on the motion of single droplet[6-8]. How to consider the phase separation phenomenon in the macro transport system, especially in the presence of the complicate solidification process, still remains an open subject.

Modeling of phase separation during solidification belongs to a multiphase problem. An encouraging multiphase volume-averaging model was developed by Beckermann's group[9-15], was further modified to study the globular equiaxed solidification by Ludwig et al[16-18]. These previous works laid the foundation for modeling the phase separation phenomenon and microstructure evolution in hypermonotectic alloys. The ideal spherical morphology of the decomposed second phase droplets permits describing more precisely the growth kinetics of the droplets, their hydrodynamic behavior (drag force), etc. On the other hand, the presence of the secondary liquid phase and the Marangoni motion of this secondary phase increase the complexity of the modeling. This paper highlights the modeling of decomposition of the secondary phase from the parent phase and the microstructure evolution.

Numerical Model

Phase definition and model assumptions

At least 4 phases appear in hypermonotectic solidification: the parent melt, the secondary liquid phase, the solidified monotectic matrix (as one phase) and the solidified secondary phase. For simplicity this model considers only two phases: the first liquid phase L_1 and the second liquid phase L_2. During monotectic reaction the monotectic matrix is transformed directly from L_1. Therefore the solidified monotectic matrix is modeled as L_1 phase in such a way that an enlarged viscosity is applied to the L_1 phase on reaching the monotectic temperature. The latent heat of the monotectic reaction is added to L_1 phase. L_2 droplets appearing at the monotectic reaction front are modeled to be entrapped in the monotectic matrix by applying a similar enlarged viscosity at or below the monotectic point. A similar approach has already been used by Ratke and co-workers[1, 19-22]. In addition to the above phase definition, following assumptions are made:

(1) Gravity induced sedimentation is modeled with Boussinesq approach;
(2) Both liquid phases have same viscosity;
(3) Eutectic reaction of L_2 is ignored;
(4) No collision and coalescence (coagulation) of droplets;
(5) Diffusion in a single droplet is infinitive, and between droplets is ignored.

Conservation equations

The conservation equations for a two-phase globular equiaxed solidification system have been described previously[16-18]. Modifications are made for hypermonotectic solidification.

Mass conservation:

$$\begin{aligned} \frac{\partial}{\partial t}(f_1\rho_1)+\nabla\cdot(f_1\rho_1\vec{u}_1)&=M_{21} \\ \frac{\partial}{\partial t}(f_2\rho_2)+\nabla\cdot(f_2\rho_2\vec{u}_2)&=M_{12} \end{aligned} \qquad (1)$$

Momentum conservation:

$$\frac{\partial}{\partial t}(f_1\rho_1\bar{u}_1)+\nabla\cdot(f_1\rho_1\bar{u}_1\otimes\bar{u}_1)=-f_1\nabla p+\nabla\cdot\bar{\bar{\tau}}_1+f_1\rho_1\bar{g}+\bar{U}_{21}-\bar{F}_M$$

$$\frac{\partial}{\partial t}(f_2\rho_2\bar{u}_2)+\nabla\cdot(f_2\rho_2\bar{u}_2\otimes\bar{u}_2)=-f_2\nabla p+\nabla\cdot\bar{\bar{\tau}}_2+f_2\rho_2\bar{g}+\bar{U}_{12}+\bar{F}_M \qquad (2)$$

where $\bar{\bar{\tau}}_1=\mu_1 f_1\left(\nabla\cdot\bar{u}_1+(\nabla\cdot\bar{u}_1)^T\right)$ and $\bar{\bar{\tau}}_2=\mu_2 f_2\left(\nabla\cdot\bar{u}_2+(\nabla\cdot\bar{u}_2)^T\right)$

The subscripts 1 and 2 in above equations stand for L_1 and L_2 phases. Decomposition, i.e. nucleation and growth (or dissolution) as well as coarsening of the L_2 phase in the parent melt, is taken into account through a mass transfer term M_{12} (=-M_{21}). $\bar{F}_M$ is the volume averaged Marangoni force on the L_2 droplets. The enthalpy and species conservation equations are described in literature[16-18].

Droplet growth and mass transfer

A 3-parameter law by Rappaz[16, 23] is employed to model the nucleation of the L_2 droplets. The droplets grow or dissolve by diffusion. The diffusion-controlled growth of a precipitate in a supersaturated matrix was described by Zener[1, 19].

$$\frac{dR}{dt}=\frac{D_1}{d_2}\cdot\frac{\Delta c}{\Delta c_d} \qquad (3)$$

The radius growth rate dR/dt of a droplet is governed by the difference between the far field concentration c_1 and the interface concentration c_1^* of L_1 phase, i.e. $\Delta c=c_1-c_1^*$. The solute partitioning at the L_1/L_2 interface is $\Delta c_d=c_2^*-c_1^*\approx c_2-c_1^*$, where c_2 is the L_2 phase concentration. D_1 is the diffusion coefficient and d_2 is the droplet diameter. When the droplet density n and an additional Avrami-factor f_1 (volume fraction of L_1 phase) are considered, the mass transfer rate M_{12} (kg/m^3/s) is expressed as:

$$M_{12}=n\cdot\pi d_2\cdot\rho_2\cdot\frac{D_1}{c_d}\cdot\Delta c\cdot f_1 \qquad (4)$$

Marangoni force and hydrodynamic resistance

When a droplet is placed in a melt having a temperature gradient ∇T, a thermocapillary convection in/around the droplet is induced (Fig. 1). The droplet surface is drawn from hotter towards the colder poles in order to lower the surface energy. The consequence is the motion of the droplet towards the hot region. This is called thermocapillary or Marangoni motion. Integration of the thermocapillary force acting on the droplet surface is defined as Marangoni force $\bar{f}_M$ (N). On a droplet having a relative velocity $\Delta\bar{u}$ with respect to the matrix, a hydrodynamic resistance or Stokes force $\bar{f}_{st}$ (N) exists. Based on Stokes-Rybczynski-Hadamard approximation, Young et al[6-8] have deduced $\bar{f}_M$ and $\bar{f}_{st}$ for single droplet.

$$\bar{f}_M=\frac{\pi d_2^2}{(1+\mu_2/\mu_1)\cdot(2+k_2/k_1)}\cdot\frac{\partial\sigma}{\partial T}\cdot\nabla T \qquad (5)$$

$$\bar{f}_{st}=2\pi d_2\cdot\mu_1\cdot\frac{1+3\mu_2/2\mu_1}{1+\mu_2/\mu_1}\cdot\Delta\bar{u} \qquad (6)$$

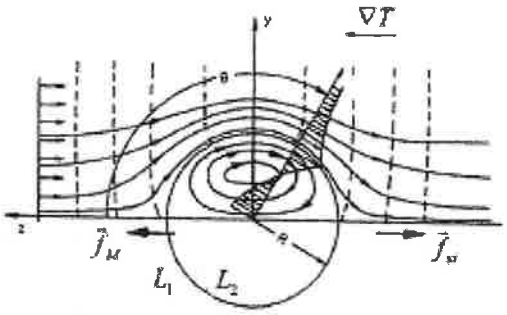

Figure 1: Thermocapillary convection in and around the droplet.

Further considering the droplet density n and the relation $f_2 = n \cdot \pi d^3/6$, the volume averaged Marangoni force $\bar{F}_M$ (N/m^3) in Eq. (2) is expressed as:

$$\bar{F}_M = \frac{6}{(1+\mu_2/\mu_1)\cdot(2+k_2/k_1)} \cdot \frac{f_2}{d_2} \cdot \frac{\partial \sigma}{\partial T} \cdot \nabla T \tag{7}$$

An empirical relationship for the Marangoni coefficient $\partial\sigma/\partial T$ is recommended[1, 19, 24],

$$\frac{\partial \sigma}{\partial T} = -1.26 \cdot \sigma_0 \cdot \frac{1}{T_c} \cdot \left(1 - T/T_c\right)^{0.26} \tag{8}$$

where σ_0 is determined experimentally.

Momentum exchange $\bar{U}_{12}(=-\bar{U}_{21})$ includes two parts: a part due to mass transfer $\bar{U}_{12}^{p}$ and a part due to Stokes force $\bar{U}_{12}^{d}$. Two situations are further considered for $\bar{U}_{12}^{p}$: decomposition (including growth and coarsening) and dissolution respectively. For decomposition, the momentum transferred from L_1 to L_2 is determined according to $\bar{u}_1$, i.e. $\bar{U}_{12}^{p} = \bar{u}_1 \cdot M_{12}$. By analogy we have $\bar{U}_{12}^{p} = \bar{u}_2 \cdot M_{12}$ for dissolution. The Stokes force is expressed as $\bar{U}_{12}^{d} = K_{12} \cdot \Delta\vec{u}$, where K_{12} can be deduced from Eq.(6).

$$K_{12} = \frac{1+3\mu_2/2\mu_1}{1+\mu_2/\mu_1} \cdot \frac{12 f_2}{d_2^2} \cdot \mu_1 \tag{9}$$

Table I: Notation of phase diagram information of Al-Bi system

Monotectic temperature	T_m	930 K	657 °C
Monotectic concentration	c_m	0.47 at. %	3.526 wt. %
L_2 monotectic concentration	c_{L2}	83.4 at. %	97.493 wt. %
Critical temperature	T_c	1310 K	1037 °C
Melting point of Al	T_f^A	933 K	660 °C
Melting point of Bi	T_f^B	543 K	270 °C
Gross concentration	c_0	1.415 at. %	10 wt. %
Slope of liquidus at c_0	m	2042.0 K	2042.0 °C
Partitioning coefficient	k	9.55	9.55

Problem description

A 2D square casting (90 x 90 mm^2) with the composition Al-10wt.%Bi is meshed into volume elements of 5x5 mm^2. The mold, remaining at a constant temperature of 290 K, is assumed to be filled simultaneously with melt of initial temperature 1065 K. The heat exchange coefficient at casting-mold interface is 750 W/(m^2.K). The nucleation parameters[23] for L_2 droplets are n_{max}= 10^{13} m^{-3}, ΔT_N = 20 K, ΔT_σ = 8 K. Other thermal physical properties and modeling parameters are listed in Table I-II.

Table II. Thermophysical properties used for the simulation[19-20, 24]

ρ = 2340 kg/m	$c_{p(2)}$ = 124.8 J/kg/K	Δh_d = 10.775 kJ/kg
k_1 = 238 W/m/K	$\mu_1 \approx \mu_2 = 1.03 \cdot 10^{-3}$ Kg/m/s	Δh_M = 383 kJ/kg
k_2 = 15.5 W/m/K	$D_1 = 1.1 \cdot 10^{-8}$ m^2/s	σ_0 = 0.1427 J/m^2
$c_{p(1)}$ = 917 J/kg/K	D_2 = 0.0	

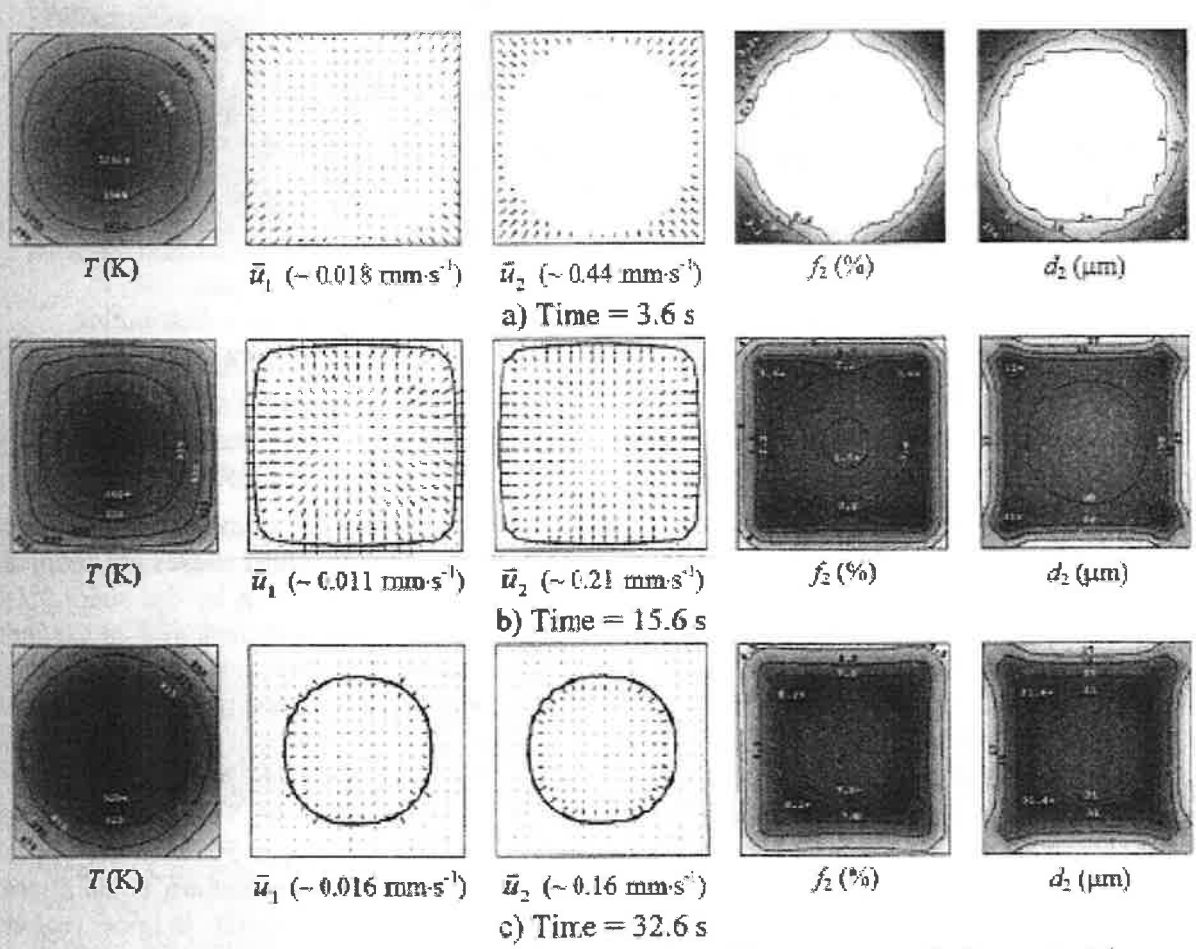

Figure 2: Solidification sequence without gravity. The arrows of the velocities are equidistantly scaled from 0 to the maximum value given, and the monotectic front (T=925 K) is drawn together with the velocity fields. Other quantities are shown with isolines together with 30 gray levels, with dark showing the highest value and bright the lowest.

Results and discussions

Without gravity

As shown in Fig. 2, phase separation, i.e. decomposition and growth with droplet motion is independent of gravity. Marangoni motion presents the only mechanism for the phase transport

in the absence of gravity. Droplets of L_2 start to nucleate and grow in the casting surface as the local temperature drops below the binodal (1062.2 K). The Marangoni force causes the L_2 droplets to move from surface region towards the casting center. The parent melt moves in reverse direction, because the space of the leaving phase L_2 must be replaced by the parent melt L_1. The movement of L_2 will definitely result in depletion of the L_2 phase (f_2) in the corners and surface regions, and enrichment of L_2 phase in the casting center. As the casting further cools down to the monotectic point, monotectic reaction occurs, the velocity of L_1 vanishes and the L_2 droplets are entrapped in the monotectic matrix. When solidification (Fig. 3) is finished the surface has a lower volume fraction of L_2 phase ($f_2 < 4.5\%$) and the center has higher volume fraction ($f_2 > 8.3\%$). The spatial separation of the phases is directly responsible for the macrosegregation: $c_{mix} < 7.2\%$Bi in corners, $c_{mix} > 12\%$Bi in center. Both Marangoni motion and diffusion controlled growth contribute to an uneven droplet size distribution. A tendency of finer droplets in the surface regions ($d_2 < 27$ μm) and relatively large droplets in the central region ($d_2 > 31.5$ μm) is predicted.

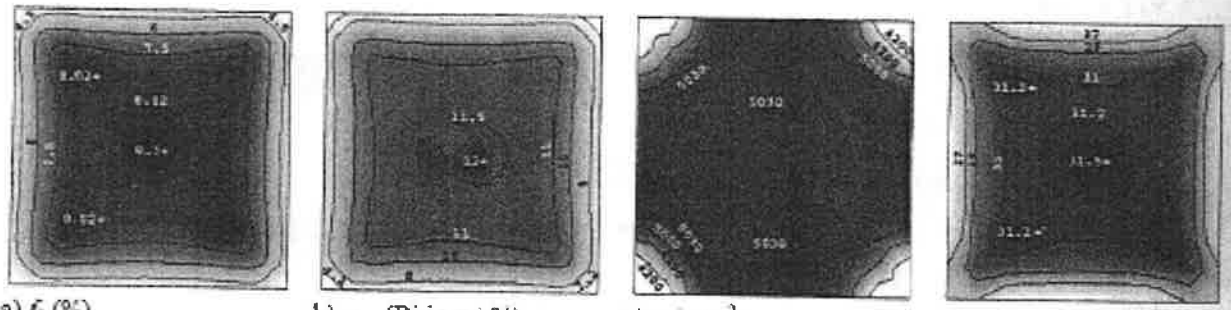

a) f_2 (%) b) c_{mix} (Bi in wt.%) c) n (mm^{-3}) d) d_2 (μm)

Figure 3: Computer-predicted phase separation, macrosegregation and droplet distribution (without gravity). All quantities are shown with isolines together with 30 gray levels, with dark showing the highest value and bright the lowest.

With gravity

As shown in Fig.4, the droplets of the L_2 phase starts to nucleate in the corners and along the walls, then grow and sink downwards along the vertical walls. As two liquid phases are coupled through the momentum exchange terms the parent melt L_1 phase is drawn by the sinking L_2 phase, forming two vortices: one clockwise in the right half and one anticlockwise in the left half of the casting. The convection currents of L_1 are so strong that they in turn influence the movement and the distribution of L_2 droplets. With the monotectic reaction the L_2 droplets are entrapped in the monotectic matrix, the phase and droplet size distribution remain unchanged afterwards. The final solidification results (Fig. 5) show the depletion of L_2 phase in the upper region ($f_2 < 2\%$) and an enrichment of L_2 in the central bottom region ($f_2 > 22\%$ L_2). Strong spatial separation of the phases leads to a strong macrosegregation: $c_{mix} < 5\%$Bi in the upper region, $c_{mix} > 25\%$Bi in the lower bottom region. The droplet distribution pattern is the direct outcome of melt convection and droplet transport. A tendency of small droplets in upper region ($d_s < 18$ μm) and large droplets in the lower bottom region ($d_s > 45$ μm) is predicted.

The convection patterns with and without g are totally different. The convection and spatial separation of the two liquid phases with g (max $\bar{u}_1 \approx 81$ mm/s) is much stronger than that without g (max $\bar{u}_1 \approx 0.44$ mm/s). Although both Marangoni motion and gravity induced droplet motion are considered in the case with g, no influence of Marangoni motion on the solidification result is seen. The function of the gravity overwhelms the Marangoni force under normal terrestrial condition as often anticipated in the experimental literature without proof[1, 3].

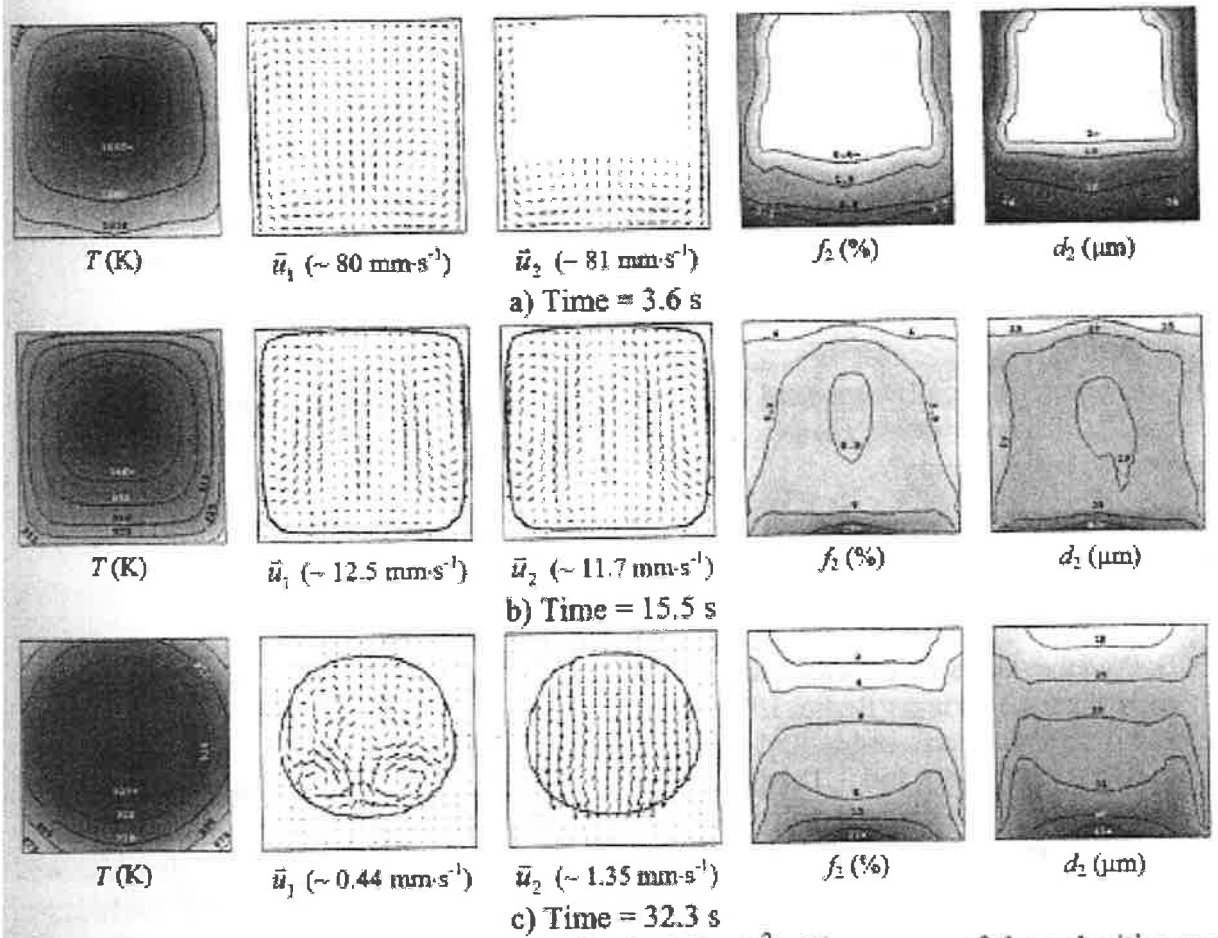

Figure 4: Solidification sequence with gravity (g=9.8 m/s^2). The arrows of the velocities are equidistantly scaled from 0 to the maximum value given, and the monotectic front (T=925 K) is drawn together with the velocity fields. Other quantities are shown with isolines together with 30 gray levels, with dark showing the highest value and bright the lowest.

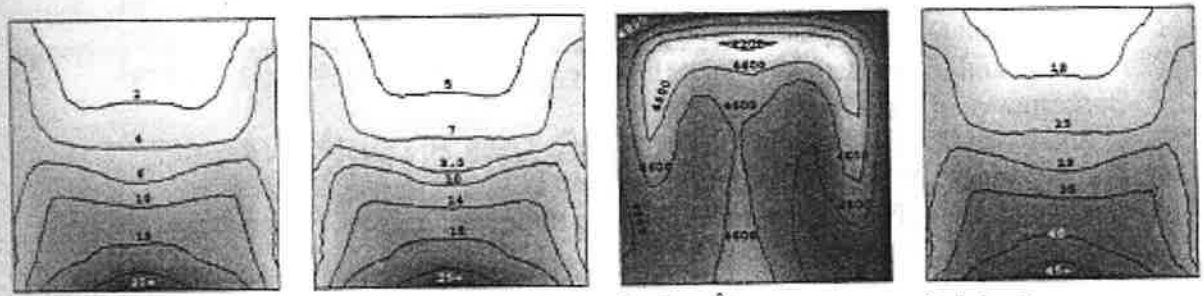

Figure 5: Computer-predicted phase separation, macrosegregation and droplet distribution (g=9.8 m/s^2). All quantities are shown with isolines together with 30 gray levels, with dark showing the highest value and bright the lowest.

Closing remarks

The modeling results demonstrate that the recent two phase model is able to simulate the decomposition and the microstructure evolution during solidification of hypermonotectic alloys. Nucleation of the secondary phase droplets, droplet growth, Marangoni motion, gravity induced phase sedimentation, parent melt convection, macrosegregation, monotectic reaction, etc. are all considered. Although the microstructure evolution in the molten state have since long been recognized in many experimental studies under both microgravity and terrestrial situations, our simulation results on the square casting have not yet been quantitatively compared with

experiment. However, the results presented in Fig. 3 agree qualitatively remarkably well with experiments performed by Walter in sounding rocket experiments using Al-Bi alloys[25] and Fig. 5 to a certain extent also with experiment performed by Alkemper and Ratke in chill cast Al-Bi alloys under terrestrial conditions[22] The recent model is established based on some modeling assumptions. The nucleation parameters used in the above simulations, for example, were empirically given. In order to evaluate the modeling results, further parameter studies or improvement on the model by releasing some modeling assumptions may be necessary.

Acknowledgement

This work was financially supported by the ESA-MAP project "Solidification Morphologies of Monotectic Alloys-MONOPHAS" and the DLR project "Simulation of the Dynamics of Monotectic Solidification".

References

1. L. Ratke, and S. Diefenbach, Mater. Sci. Eng., 15(R)(1995), 263-347.
2. B. Predel et al., in H. U. Walter and M. F. Ashby (eds.), Decomposition of Alloys: The early Stages, (Springer Berlin, 1987), 517-565.
3. B. Prinz, A. Romero, and L. Ratke, J. Mater. Sci., 30(1995), 4715-4719.
4. L. Ratke, G. Korekt, and S. Drees, Adv. Space Res., 22(1998), 1227-1236.
5. L. Ratke, and G. Korekt, Z. Metallkd., 91(2000), 919-927.
6. N. O. Young, J.S. Goldstein, and M. J. Block, J. Fluid Mech., 6(1959), 350-356.
7. W. Günter, Über die Dynamik von Fluidpartikeln aufgrund des Marangoni-Effektes, (Düsseldorf: VDI-Verlag, 1993).
8. M.G. Velarde, in L. Ratke, H. Walter, B. Feuerbacher (Eds.), Materials and Fluids under Low Gravity, (Springer Berlin, 1995), 283-298.
9. C. Beckermann, and R. Viskanta, Appl. Mech. Rev., 46(1993), 1-27.
10. J. Ni, and C. Beckermann, Metall. Trans. B, 22B(1991), 349-361.
11. C.Y. Wang, and C. Beckermann, Metall. Mater. Trans. A, 27A(1996), 2754-2764.
12. C.Y. Wang, and C. Beckermann, Metall. Mater. Trans. A, 27A(1996), 2765-2783.
13. C.Y. Wang, and C. Beckermann, Metall. Mater. Trans. A, 27A(1996), 2784-2795.
14. C. Beckermann, JOM, 49(1997), 13-17.
15. A.V. Reddy, and C. Beckermann, Metall. Mater. Trans. B, 28B(1997), 479-489.
16. A. Ludwig and M. Wu, accepted for publication in Met. Trans A, 2002.
17. M. Wu, A. Ludwig, P.R. Sahm, and A. Bührig-Polaczek, in D.M. Stefanescu et al (Eds.): Proceeding of MCWASP X, 2003.
18. M. Wu, A. Ludwig, A. Bührig-Polaczek, M. Fehlbier, and PR. Sahm, submitted to Inter. J. Heat Mass Transfer, (2002).
19. S. Diefenbach, "Modellierung der Gefügeentwicklung von Monotekta" (Ph.D. thesis, Ruhr-University Bochum, 1993).
20. L. Ratke et al., in L. Ratke, H. Walter, B. Feuerbacher (eds.), Materials and Fluid under Low Gravity, (Springer Berlin, 1995), 115-133.
21. J. Zhao, L.Ratke, Z. Metall., 89 (1998), 241-246.
22. J. Alkemper, L. Ratke, Z. Metall. 85 (1994), 365-371.
23. M. Rappaz, Int. Mater. Rev., 34(1989), 93-123.
24. F. Falk, in L. Ratke (eds.), Immiscible Liquid Metals and Organics, (DGM Informationsgesellschaft mbH, 1993), 93-100.
25. H. U. Walter, in Järva Krog (eds.), Proc. RIT/ESA/SSC Workshop, ESA SP 219, (Noordwijk, Sweden, 1984), 47-64.